SPECTRAL PROFILES COMPARISON OF *CANDIDA GUILLIERMONDII* AND *CANDIDA KRUSEI* YEASTS CELLS

Raluca D. NEGOITA[1], Nicoleta A. MIN[2]*, Marcela POPA[3], Carmen M. CHIFIRIUC[3, 4], Mona MIHAILESCU[5]

Hyperspectral imaging has emerged as a powerful tool enabling the analysis of spectral signatures at cellular and subcellular levels. In this study, we applied enhanced dark-field hyperspectral microscopy to compare two Candida species—C. guilliermondii and C. krusei—using ascospore-stained smears. Spectral profiles (SPs) were extracted for morphological compartments: cytoplasm, acospores, cell wall boundary, bud scars, buds, and free spores. Each SP was analyzed both as an 1D function and as a high-dimensional vector. We computed quantitative features including areas under the curves and under their first derivatives, vector-based metrics such as angles and distances. Statistical analysis revealed that features derived from the SPs first derivative provided significant discrimination between the species ($p < 0.05$), especially for the spore. Moreover, vector-based comparisons showed highly significant differences ($p < 0.0005$) between the spore regions of the two species. These results suggest that spores may exhibit species-specific optical properties, making them strong candidates for automated classification. This work demonstrates that simple, yet robust features extracted from hyperspectral profiles can support the differentiation of Candida species and could serve as input for future machine learning algorithms for microbial identification.

Keywords: Candida guillermondii, Candida krusei yeasts, hyperspectral images, spectral profiles, free spores, vectors.

1. Introduction

In recent years, the taxonomy of pathogenic *Candida* species has been complicated due to the description of new closely-related species, which are difficult to discriminate in clinical diagnostic laboratories with currently available phenotypic methods. These challenges have been partially overcome by the

[1] Phd stud. Applied Sciences Doctoral School, National University of Science and Technology POLITEHNICA Bucharest, Romania, raluca.negoita@upb.ro
[2] Ms stud., Faculty of Medical Engineering, National University of Science and Technology POLITEHNICA Bucharest, Romania, nicoleta.potirniche@stud.fim.upb.ro *Corresponding author
[3] Research Institute of the University of Bucharest, University of Bucharest, Romania
[4] Biological sciences Division, Romanian Academy, Bucharest Romania
[5] Prof., Physics Dept, Research Center for Applied Sciences in Engineering, National University of Science and Technology POLITEHNICA Bucharest, Romania.

development of PCR-based and MALDI-TOF methods [1]. However, these approaches are often sophisticated, requiring cultivation and isolation of the yeast strains in pure culture and the utilization of toxic chemicals. Therefore, there is a need for fast, reliable, and inexpensive methods with high specificity for the identification and differentiation of pathogenic *Candida* species.

Hyperspectral images (HSI), by capturing both spatial morphology and rich spectral profiles, enables distinguishing microbial species based on their unique "optical fingerprints". In addition to classical optical microscopy techniques, hyperspectral dark field microscopy provides additional information, through spectral profiles over a wide range of wavelengths, with pixel-level resolution, allowing for more complex analysis. For example, the *Staphylococcus aureus* strains were identified with 93.9% accuracy using SVM models using thirty-one spectral bands extracted from HSI [2]. An early detection procedure for *Salmonella* serotypes was proposed using principal component analysis and Mahalanobis distance starting from HSI [3]. A comparative study investigated the foodborne pathogens *Salmonella spp*, *Escherichia coli* and *Listeria spp* at 18, 21 and 24 hours of growth, with HSI facilitating the finding of single-peak spectral profiles that can be analyzed by simple computer methods, in contrast to conventional ones that require spectral convolution [4]. Two *Gram-positive bacteria* were differentiated from a mixture using HSI and machine learning based on the observation that there is a difference in their pH, detectable by spectral profiles (SPs) [5].

A mid-infrared HSI system using quantum cascade lasers was introduced to image microbial colonies (including fungi like *Candida albicans*) at multiple wavelengths. This morpho-spectral approach correctly identified ~94% of colonies, even discriminating closely related strains, all without staining or culturing beyond colony formation [6]. Similarly, *in situ* spectral analyses of microorganisms have achieved high accuracy, near-infrared spectroscopy and HSI being able to classify anaerobic gut fungi into three genera with >95% accuracy using discriminant analysis[7]. These results underscore that different microbes exhibit characteristic spectral signatures (due to variations in cell wall composition, pigments, etc.), which HSI can exploit for identification. Notably, pathogenic yeasts of the genus *Candida* have been a focus in some HSI applications. For instance, *C. albicans* and C. *tropicalis* were successfully detected in a clinical context via HSI of urine smears, alongside bacteria, demonstrating HSI's potential in rapid fungal diagnostics[8]. Overall, recent literature supports that HSI, when coupled with appropriate analysis, offers a fast and non-destructive means to identify microbes at early stages, addressing the long turnaround of culture-based methods [9,10].

Combination between HSI and machine learning allows automated analysis using spectral criteria to: determine quality of food [11], to classify neurons and glia in neural stem cell cultures [12], to classify irradiated nuclei [13], to detect

bacterial, fungal and viral contaminants in food [14] or to compute distances between three species [15].

The objective of our study was to test the hypothesis that HSI can provide useful information regarding the characteristics of two *Candida* species allowing to differentiate them and thus improve their automatic classification. For this, we recorded hyperspectral images for *C. guillermondii* (CGY) and *C. krusei* (CKY) yeasts smears stained by the specific ascospores staining.

For both types of yeasts, we selected separate spectral profiles (SP) for morphological components: cytoplasm (C), ascospores (A), cell wall boundary (CWB), bud scars (BS), buds (B), and free spores (FS). These components are essential to characterize and compare these cell types.

In our analysis, SPs were viewed both as I(λ), 1D functions (intensity in each spectral band) and also as vectors with 468 elements (corresponding to each band between 400 nm and 1000 nm). For SPs functions, we computed areas under curves and their derivatives; in vector space, the computation of angles and distances between vectors was performed. These features were computed both between components of a single species and between species. We chose to test the significance of these types of features because the standard ones (texture, roughness) are not possible here due to the very small areas occupied by each component in the image.

2. Experimental procedures

2.1 Samples preparation

To induce sporulation, yeast strains from the collection of the University of Bucharest, Faculty of Biology, Microbiology Department were subcultured through three successive passages on malt extract agar, incubated at 28°C, with transfers performed at 24-hour intervals. Following the final incubation, the supernatant was carefully removed using a sterile Pasteur pipette, and the resulting dense cellular sediment was collected. Using a sterile Pasteur pipette, aliquots of the sediment were deposited in small spots onto the surface of sterile Petri dishes containing sporulation medium. The inoculated plates were then incubated at room temperature (22–28°C), in the dark, for a period ranging from 2 to 7 days to promote ascospore formation. For microscopic examination, smears were prepared from the sporulated spots by gently spreading a small amount of material onto clean glass slides. The smears were allowed to dry air at room temperature and were subsequently heat-fixed by briefly passing the slides through a flame. Staining was performed using a modified ascospore staining technique. The heat-fixed smears were stained with a 1:10 dilution of basic fuchsin solution, applied under gentle heating for 2–3 minutes (with 2–3 steam emissions to enhance penetration). Slides

were then rinsed thoroughly with tap water and decolorized using a mixture of 0.1N hydrochloric acid and ethanol in a 2:1 (v/v) ratio for 30 seconds. After another rinse with tap water, counterstaining was performed using 1% methylene blue solution for 1–2 minutes. A final rinse with tap water was followed by air drying at room temperature [16].

2.2 Images acquisition and preprocessing

Hyperspectral images under enhanced darkfield microscopy were recorded using CytoViva^{R} commercial system which allows obtaining images with a very dark background thanks to an oil-immersed condenser that ensures illumination of the sample at a very oblique angle. Hyperspectral images containing in each pixel information about intensity on 468 spectral bands between 400 nm and 1000 nm wavelengths were obtained by scanning the sample in the XY plane with a motorized stage (NanoScanZ, Prior Scientific Instruments Ltd, UK, 10 nm step size, 114 × 75 mm travel range). From this reason, each image is considered as a spectral data cube (x, y, λ) (696x696x468).

The system is equipped with a spectrophotometer (ImSpectrum V10E, Specim Finland) containing a transmission diffraction grating inserted between the objective and a hyperspectral camera (Pixelfly 1392 × 1040-pixel resolution, 6.45 × 6.45 µm pixel size, 7.3 to 13.5 fps, 5 µs-60 s exposure time range, 62% quantum efficiency). Other constructive and operational details are in [17].

Hyperspectral images for each of the studied yeast species are recorded with 100x microscope objective and are presented in Fig. 1.

a) 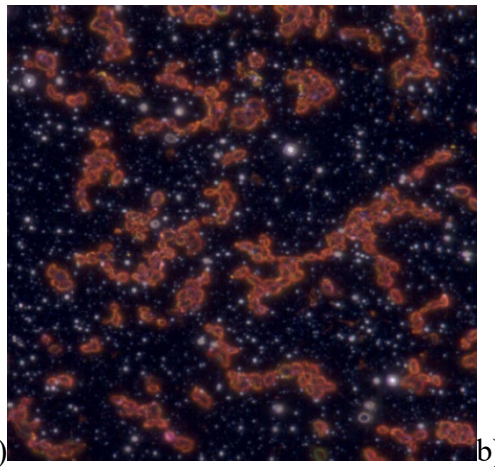 b) 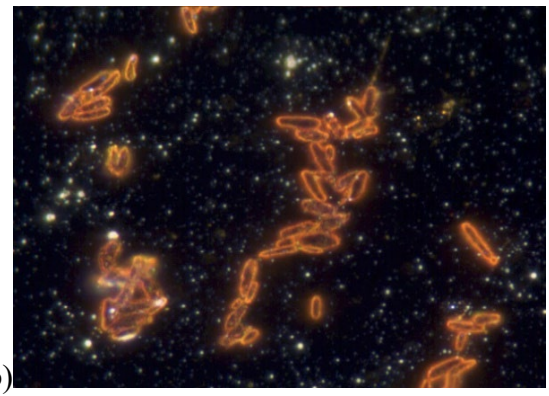

Fig. 1. Experimental hyperspectral images for a) CGY and b) CKY.

Using the specialized software ENVI [18], spectral profiles (SPs) can be viewed at the pixel level, averages over 3x3 neighboring pixels or averages over a

region of interest chosen by the user. We saved in the spectral library specific SPs for all morphological components of the two yeast species (cytoplasm, ascospores, cell wall boundary, bud scars, buds, and free spores).

3. Results and discussions

3.1. Spectral profiles

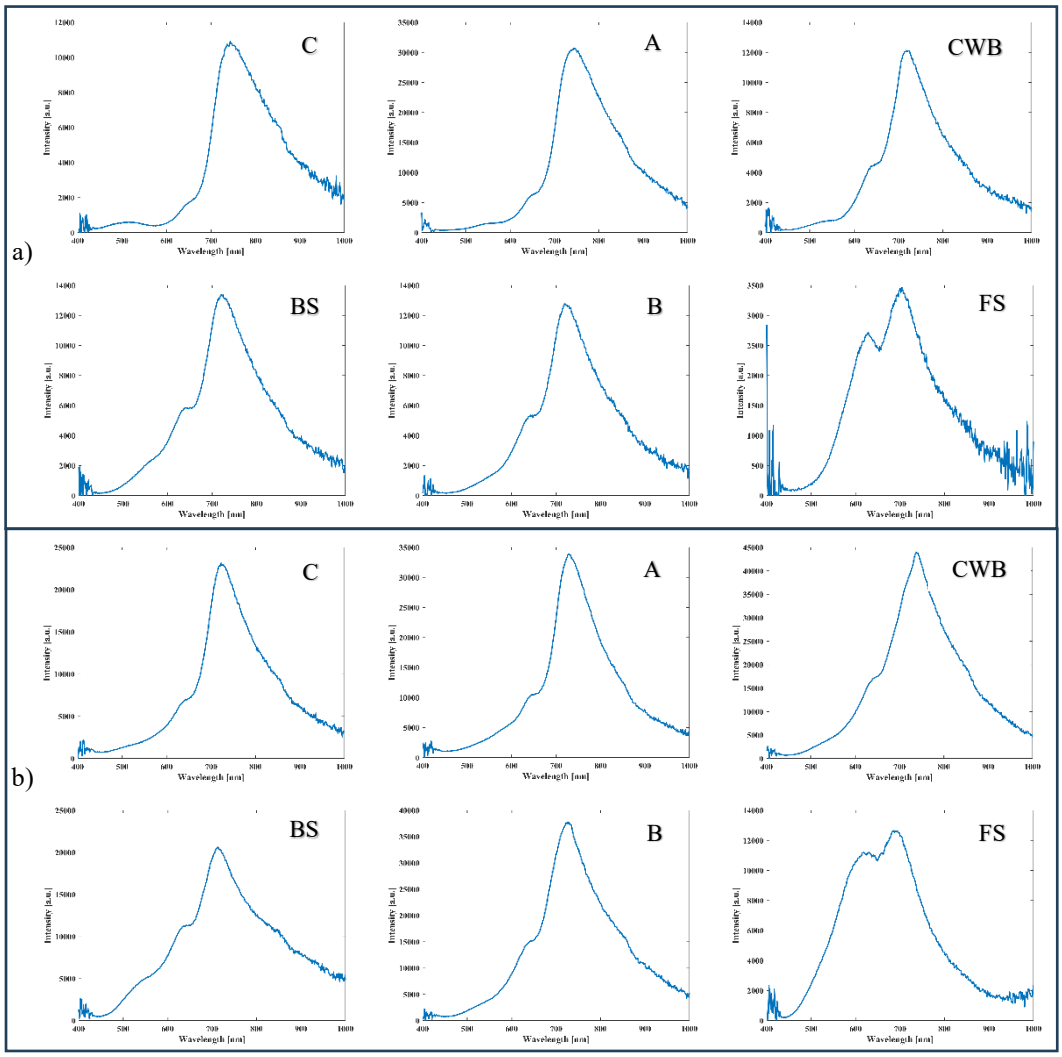

Fig. 2. Spectral profiles for each compartment from a) CGY, b) CKY.

In our study we used SPs displayed in ENVI as averages on 3x3 pixels. In the Fig. 2 are represented separately SPs for each analized yeast (CGY and CKY)

on morphological compartments: cytoplasm (C), ascospores (A), cell wall boundary (CWB), bud scars (BS), buds (B), and free spores (FS).

All these spectral profiles have a steep maximum in the spectral range 700-750nm, shifted towards the lower border for the spore and cell wall boundary and towards the upper border of the range for the ascospore. For the spore compartment, for both yeast species investigated, the secondary maximum appears more pronounced around 625 nm. For budding scars, the third maximum is also visible around the spectral band of 550nm (more evident for CKY). By simple visual observation, these SPs are hard to be differentiated and for this reason, we computed features based on mathematical rules from functions and vectors. We collected ten SPs from each category from Fig. 2 and computed the features from SPs function (areas under curve and its first derivative) and SPs vector (angles, distances).
All these SPs are normalized and considered as inputs for our home-made code in MATLAB. From an SP we consider three entities: SP, its first derivative, SP-vector with 468 elements to compute spectral features: areas under curves, angles, distances. Normalization was performed in respect to intensity values from the spectral profiles, computing the rations between each intensity value (at each spectral band) and the maximum value in that SP. In this king, each SP will have intensity values between 0 and 1 to compensate for any artifacts that may appear in the experimental procedures: non-uniform staining with chromatographic marker, different illumination from image to image or from sample to sample during experimental image recording.

3.2. SP functions

SPs were saved from ENVI software and imported in MATLAB. They are 1D functions: $I(\lambda)$, the intensity values for each spectral band between 400-1000 nm. A home-made code computed the values of the areas under the curve and its first derivative (Fig. 3) for each morphological component of the two *Candida* species. We worked with normalized values for SPs. The areas under spectral curves (or spectral curves derived) are considered as cumulated sums of intensity values (or derived intensities) on the whole spectral interval 400 - 1000 nm. We selected to analyze the first derivative of the SPs because it emphasizes significant spectral intensity variations, effectively highlighting the wavelengths where sharp spectral changes occur.

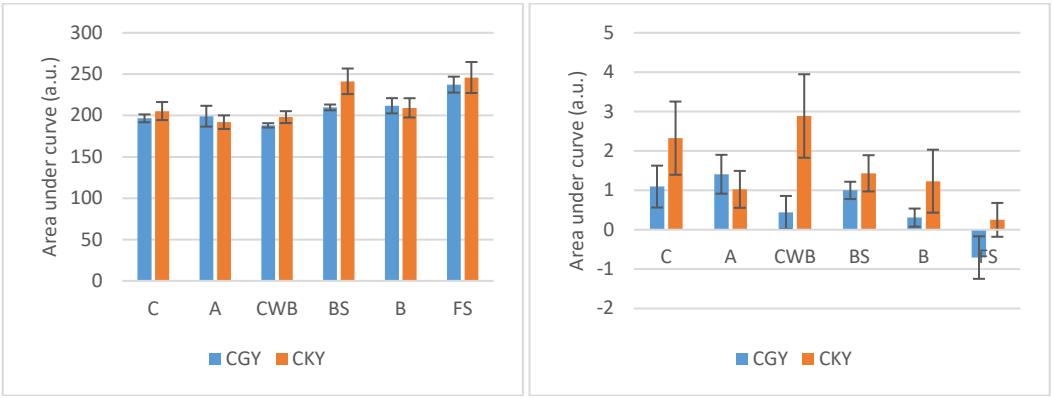

a) b)

Fig. 3. Areas under a) SPs and b) derived SPs considered as curves.

An ANOVA test was performed on two datasets: the area under the original SP curves and the area under their first derivatives. The analysis yielded a p-value of < 0.5 for the original curves, indicating no statistically significant difference between *C. guilliermondii* (CGY) and *C. krusei* (CKY). In contrast, the derivative-based curves produced a p-value < 0.05, suggesting a statistically significant distinction between the two species.

These findings support the general observation that the original spectral profiles exhibit similar overall trends for CGY and CKY, whereas their derivatives reveal more distinct patterns. Based on this result, we propose that the area under the derivative of the SP curve may serve as a discriminative feature for distinguishing between the two yeast species, particularly when analyzing the cell wall boundaries, bud, and free spore compartments.

3.3. SP vectors

The SP values in each spectral band between 400 and 1000 nm can be considered as forming a vector with 468 values. In this way, we will have ten vectors that characterize each component of the two *Candida* species of candida yeasts. The in-house developed MATLAB code computed four features to characterize the differences/similarities between the components of the species: 1/ angles between SP vectors associated with the same type of component from the two species, 2/ angles between SP vectors associated with components of different types from the same species, 3/ distances between SP vectors associated with the same type of component from the two species, 4/ distances between SP vectors associated with components of different types from the same species. Figs. 4 and 5 represent the analysis of all these features. The larger the values of the angles and distances, the more dissimilar the two species/compartments are.

From the Fig. 4 a) we can observe that angles above 0.2 rad between the same compartment from the two species, are only for cytoplasm and free spores. From the Fig. 4 b) and c) we can observe that the spores have the largest values for angles computed besides all other compartments for the same species. The same observation also from the Fig. 5 b) and c): the free spores have the highest distances computed against all other compartments belonging to the same species.

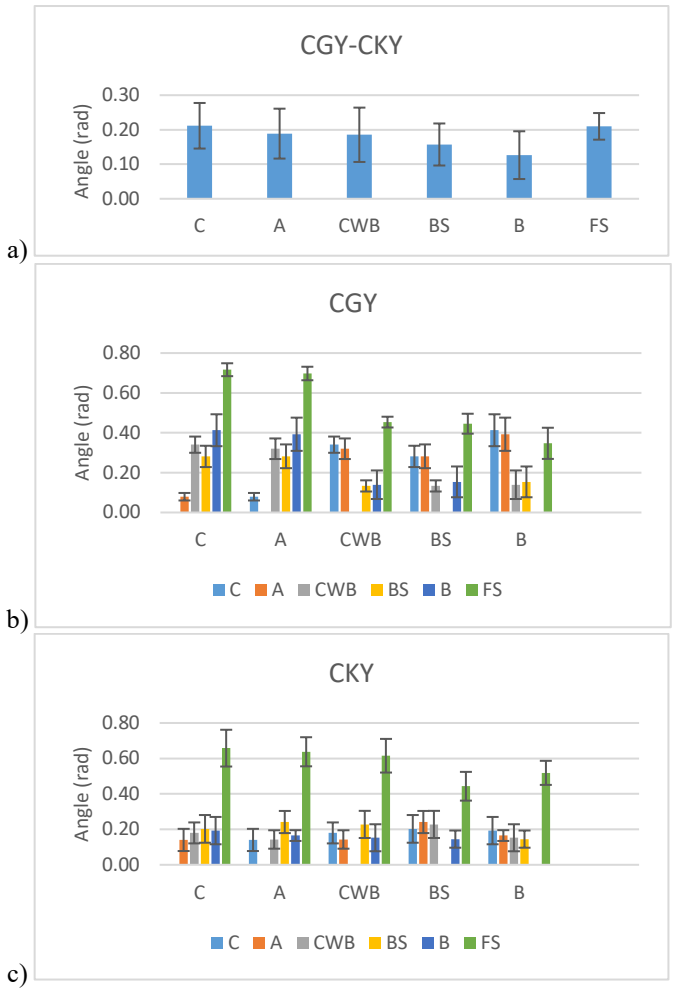

Fig. 4. Angles between SP vectors associated with a) the same type of component from the two species, b) components of different types, from CGY, c) components of different types, from CKY.

The ANOVA tests performed on the data presented in Fig. 4 yielded highly significant results ($p < 0.0005$) when comparing the angles between spectral profile (SP) vectors of the free spore compartment and those of other compartments, as opposed to comparisons between non-spore compartments. A similar level of

significance ($p < 0.0005$) was observed for the distances represented in Fig. 5. These findings suggest that the spore compartment exhibits distinctly different spectral behavior relative to other cellular structures. Biologically, this supports the hypothesis that the spore region may contain species-specific biochemical or structural features —such as variations in wall composition or pigment accumulation— which result in differentiable spectral signatures. Therefore, spectral features derived from the spore compartment may serve as valuable discriminative markers for automated species identification between *C. guilliermondii* and *C. krusei*.

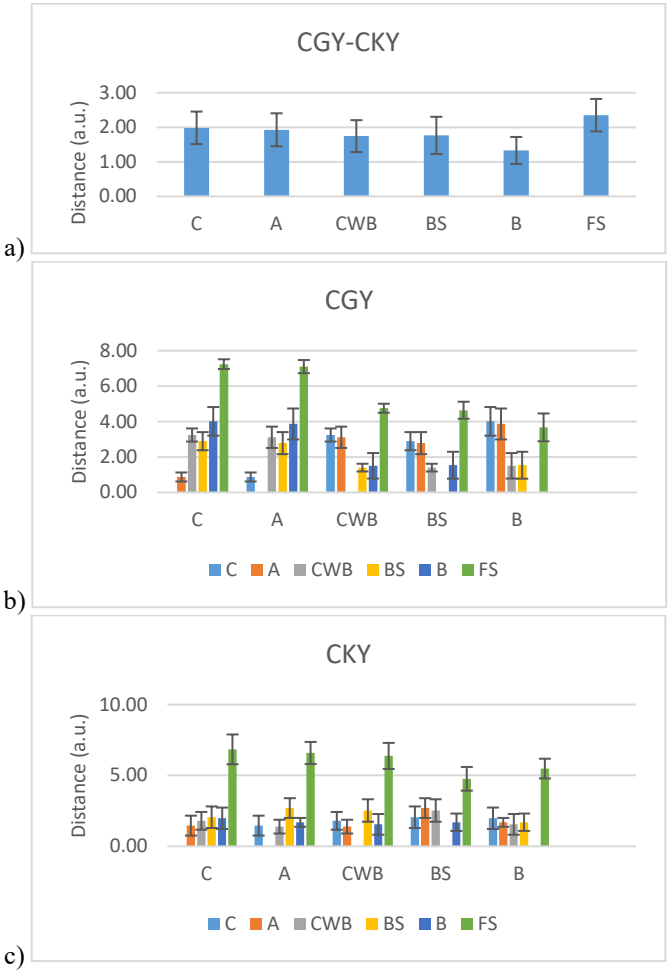

Fig. 5. Distances between SP vectors associated with a) the same type of component from the two species, b) components of different types, from CGY, c) components of different types, from CKY.

Starting from the first derivate of the SP functions, we associated the vectors and computed the same features: 1/ angles between SP vectors associated with the

same type of component from the two species, 2/ angles between SP vectors associated with components of different types from the same species, 3/ distances between SP vectors associated with the same type of component from the two species, 4/ distances between SP vectors associated with components of different types from the same species (Figs. 6 and 7).

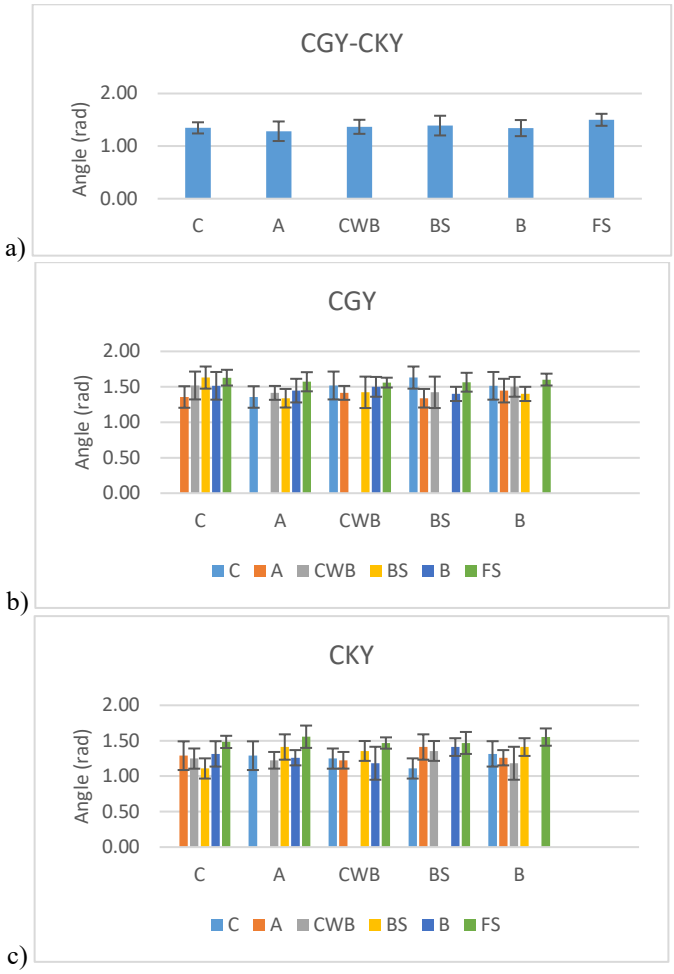

Fig. 6. Angles between SP derivative vectors associated with a) the same type of component from the two species, b) components of different types from CGY, c) components of different types from CKY.

We can observe in Fig. 6 a) that there is no angle above 0.2 radians, so this feature cannot be used to highlight the differences between yeast species. The same behavior is observed in Fig. 6 b) and c) for the angles computed between different compartments of the same species. For distances, the one computed between the vectors from the derivative of the SP function, corresponding to the edges CGY and

CKY is 1.5 times greater than those calculated for cytoplasm, ascospores, bud and free spore. Distances computed between vectors from the SP derivative function associated with components of different types from CGY and from CKY have very close values; they do not represent features that differentiate between the investigated yeasts species.

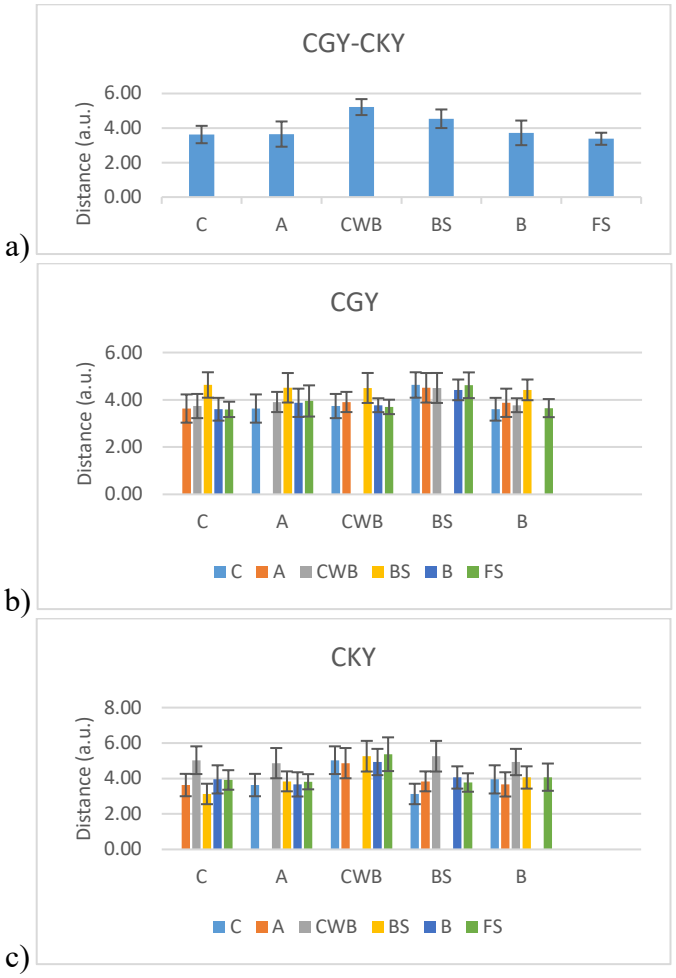

Fig. 7. Distances between SP derivative vectors associated with a) the same type of component from the two species, b) components of different types, from CGY, c) components of different types, from CKY.

The findings from our spectral comparisons of *C. guilliermondii* and *C. krusei* can be contextualized by recent HSI studies on microbial identification. High accuracy rates reported in the literature bolster the significance of any spectral differences we observed between these two *Candida* species. For instance, our work resonates with the 2024 report of Neurauter *et al.*, who achieved >95% accuracy differentiating fungal genera via HSI [7]. While their study dealt with anaerobic gut

fungi, the principle is similar – microbial taxa can be robustly distinguished by their spectral "fingerprint," supporting our approach. Moreover, the successful identification of *C. albicans* in mixed samples by mid-IR HSI and in clinical smears suggests that *Candida* yeasts have discernible spectral signatures [6]; our results extend this knowledge to *C. guilliermondii* and *C. krusei*, two non-albicans species of clinical interest. On the other hand, if the spectral differences we found are subtle, literature still offers strategies to amplify or interpret them. For example, Liu *et al.* (2023) improved fungal classification by moving to the SWIR range and applying advanced preprocessing, implying that certain spectral ranges or normalization techniques might enhance species distinctions [19].

The success of deep learning models (94–99% accuracy) in classifying single bacterial cells from HSI suggests that even higher accuracy might be achievable for yeast identification as more data are gathered. Indeed, Tao *et al.* [10] demonstrated a genus-level bacteria classifier with 94.9% accuracy by training on 130,000+ spectral images and deploying a custom CNN ("Buffer Net"). While our dataset is smaller, our results contribute to this growing evidence that HSI combined with automated features computation is a viable path for rapid yeast identification and a starting point for ML classification. We note that unlike some colony-based HSI methods that still require growth on plates, our dark-field microscopic HSI can potentially identify *Candida* at the single-cell level, reducing the time to result. This advantage is frequently cited as crucial for timely antifungal therapy. Finally, we consider how our findings could be applied or extended. The literature points toward integrating HSI with clinical workflows. In light of this, the spectral differences we document between *C. guilliermondii* and *C. krusei* could be used to train detection algorithms in similar diagnostic HSI systems.

2. Conclusions

We computed features to evaluate the differences/similarities among the properties of two *Candida* species starting from SP. First, we considered SP as functions and computed the areas under the curves and its first derivative for each component from both species of candida yeasts. Then, we associated vectors with the two functions and computed angles and distances between the vectors of each component from the two species and between each component of the same species. Our goal was to find those features, simple to be computed, that would allow further automated identification of the two species based on single-cell analysis.

Among the features investigated, those that are significant in highlighting the differences between the compartments of the two species are: 1/ the area under the SP derivative curve, 2/ the angles between SP vectors and 3/ the distances between SP vectors. Significant statistical distinctions between the optical properties of two species are observed in the case of areas under derivative curves

($p<0.05$), and when comparing the angles and distances between SP-vectors of the free spore compartment and those of other compartments ($p < 0.0005$).

Finding relevant features is a challenge in automatic classification, as it has been proven that the values of the evaluation metrics of the supervised machine learning algorithms change depending on the input data. For the task of automated pathogen identification, hyperspectral images have proven to be a powerful tool that contain information about the chemical composition of samples, and spectral profiles are easy to use in features computation. In conclusion, the technique has potential for future use in combination with machine learning and deep learning algorithms.

Acknowledgement

MCC acknowledges the support of CNFIS-FDI-2025-F-0364. The research is partially supported by the grant Advanced Infrastructure for Nuclear Photonics research experiments at ELI-NP / ELI-INFRA through the national research and development program PNCDI IV / 5.9.1 ELI-RO: ELI-NP infrastructure development projects. The hyperspectral images were recorded using CytoViva system acquired through INOVABIOMED Project No. P_36_611, MySMIS code 107066.

R E F E R E N C E S

[1] *G. Criseo, F. Scordino & O. Romeo*, Current methods for identifying clinically important cryptic Candida species. Journal of Microbiological Methods, Vol.**111**, Pp. 50-56, 2015.

[2] *Y. Seo, B. Park, A. Hinton, S. C. Yoon & K. C Lawrence,* Identification of Staphylococcus species with hyperspectral microscope imaging and classification algorithms. Journal of Food Measurement and Characterization, Vol.**10**, Pp. 253-263. 2016.

[3] *M. Eady, B.Park & S. U. N.Choi,* Rapid and early detection of Salmonella serotypes with hyperspectral microscopy and multivariate data analysis. Journal of Food Protection, Vol.**78(4)**, Pp.668-674, 2015.

[4] *R. D Riggs, I. H. Chen, O. Pustovyy, B. Zinner, I. Sorokulova & V. Vodyanoy,* Hyperspectral imaging of a single bacterial cell, 2020.

[5] *K. Liu, Z. Ke, P. Chen, S. Zhu, H. Yin, Z. Li & Z. Chen*, Classification of two species of Gram-positive bacteria through hyperspectral microscopy coupled with machine learning. Biomedical Optics Express, **Vol. 12(12)**, Pp.7906-7916, 2021.

[6] *J. Le Galudec, M. Dupoy, L. Duraffourg, V. Rebuffel, P. R. Marcoux,* Microbial Identification Through Multispectral Infrared Imaging of Colonies: A New Type of Morpho-Spectral Fingerprinting. Microb Biotechnol.; Vol. **18(2),** e70093, 2025, doi: 10.1111/1751-7915.70093.

[7] *M. Neurauter, J. M. Vinzelj, S. F. Strobl, C. Kappacher, T. Schlappack, J. Badzoka & S. M. Podmirseg*, Exploring near-infrared spectroscopy and hyperspectral imaging as novel characterization methods for anaerobic gut fungi. FEMS microbes, Vol.5, xtae025, 2024.

[8] *J. Du, C. Tao, M. Qi, B. Hu & Z. Zhang*, Rapid Determination of Positive–Negative Bacterial Infection Based on Micro-Hyperspectral Technology. Sensors, Vol. **24(2)**, Pp. 507, 2024.

[9] *G. Pezzotti, M. Kobara, T. Asai, T. Nakaya, N. Miyamoto, T. Adachi & K. Makimura,* Raman imaging of pathogenic Candida auris: Visualization of structural characteristics and machine-learning identification. Frontiers in microbiology, Vol. **12**, Pp.769597. 2021.

[10] *C. Tao, J. Du, Y. Tang, J. Wang, K. Dong, M. Yang & Z. Zhang,*. A deep-learning based system for rapid genus identification of pathogens under hyperspectral microscopic images. Cells, Vol. **11(14)**, Pp. 2237, 2022.

[11] *D. Saha & A. Manickavasagan*, Machine learning techniques for analysis of hyperspectral images to determine quality of food products: A review. Current Research in Food Science, Vol. **4**, Pp. 28-44, 2021.

[12] *H. Ogi, S. Moriwaki, M. Kokubo*, et al. Label-free classification of neurons and glia in neural stem cell cultures using a hyperspectral imaging microscopy combined with machine learning. Sci Rep 9, Vol. **633**, 2019, https://doi.org/10.1038/s41598-018-37241-y.

[13] *R. D. Negoita, M. A. Ilisanu, I. N. Irimescu, R. C. Popescu, M. Tudor, M. Mihailescu, E. N. Scarlat, A. M. Pleava, A. Dinischiotu & D. Savu*, Specific spectral sub-images for machine learning evaluation of optical differences between carbon ion and X ray radiation effects. Heliyon, Vol. **10(15),** e35249, 2024. https://doi.org/10.1016/J.HELIYON.2024.E35249

[14] *A. Soni, Y. Dixit, M. M. Reis & G. Brightwell*, Hyperspectral imaging and machine learning in food microbiology: Developments and challenges in detection of bacterial, fungal, and viral contaminants. Comprehensive Reviews in Food Science and Food Safety, Vol. **21(4)**, Pp. 3717-3745, 2022.

[15] *N. Tarba, N. I. Irimescu, A. M. Pleava, E. N. Scarlat, M. Mihailescu*, Distance between species by confusion operators of multi-class classifiers, U.P.B. Sci. Bull., Series A, Vol. **87(1)**, Pp.171–182, 2025.

[16] *V. Lazar, V. Herlea, R. Cernat, M. C. Balotescu, D. Bulai, A. Moraru,* Microbiologie generala, Ed. Univ, Buc., 2004.

[17] *M. Mihailescu, L. C. Miclea, A. M. Pleava, N. Tarba, E. N. Scarlat, R. D. Negoita, M. G. Moisescu & T. Savopol,* "Method for nanoparticles uptake evaluation based on double labeled fluorescent cells scanned in enhanced darkfield microscopy," Biomed. Opt. Express 14, 2796-2810, 2023.

[18] https://cytoviva.cn/wp-content/uploads/2021/pdf/CytoViva-User-Manual_10022020.pdf

[19] *Z. Liu, M. Al-Sarayreh, Y. Li & Z. Yuan,* Classification of tree symbiotic fungi based on hyperspectral imagery and hybrid convolutional neural networks. Frontiers in Forests and Global Change, Vol. **6**, 1179910, 2023.